# Supporting Information

## Chen et al. 10.1073/pnas.1715059115

### SI Adult Cardiac Fibroblast Isolation and Culture

We euthanized Sprague–Dawley rats (6 wk old, ∼220 g), removed and minced their ventricles into ∼1-mm$^3$ pieces, and digested the pieces using Liberase TM Research Grade (Roche). We centrifuged successive digestions for 10 min at 400 × *g*; resuspended the cells in culture medium containing DMEM (Sigma-Aldrich) with 10% FBS (Atlanta Biologicals), 100 U/mL penicillin, 100 μg/mL streptomycin, and 2 ng/mL amphotericin B (all Sigma-Aldrich); and transferred the cells into cell culture flasks incubated at 37 °C and 5% $CO_2$. After 4 h, we removed the culture media, rinsed the cells with PBS (Sigma-Aldrich) to remove nonadherent cells, and resupplied with culture medium. We replaced media every 2–3 d and harvested cells for experiments at passage 1 (7 d after isolation) or 2 (10–11 d after isolation).

### SI Fabrication of Fibroblast-Populated Collagen Hydrogels

We serum-starved the fibroblasts for 18 h before using 0.25% Trypsin-EDTA (Sigma-Aldrich) to dissociate them from their flasks and resuspending them in serum-free culture media. We created collagen solution at a 1:1:8 ratio of 0.2 M Hepes, 10× MEM (both Sigma-Aldrich), and 3.1 mg/mL type I Bovine Collagen Solution (PureCol; Advanced Biomatrix) and mixed it at a 4:1 ratio with the resuspended cells for a final cell concentration of 200,000 cells per 1 mL and collagen concentration of ∼2 mg/mL We placed this cell plus collagen mixture on a rotator in an incubator for 20–30 min to initiate gelation before pouring it into 100 × 15-mm Petri dishes coated with polydimethylsiloxane (PDMS; Sylgard 184 Silicone Elastomer Kit; Dow Corning) to prevent adhesion and fitted with negative cruciform molds with small sponges at the arms (Fig. 1*A*). After the gels polymerized for 4 h in an incubator, we either isotropically constrained them for 1 d by pushing two small pins through each sponge into the PDMS layer or let them float freely in media and isotropically compact for 1 d. The free-floating gels were cast from a larger total volume in larger molds to allow for compaction, so that dimensions of all gels would be matched after 1 d before transfer to the loading system.

### SI Comparison of Cell Alignment with SF Alignment

Our experiments quantified the orientation distribution of populations of cells, while most models (including the one used here; see below) predict distributions of SFs within a single hypothetical cell. To understand any differences between these two metrics that might confound interpretation, we imaged 10 cells from each 72-h loading condition (60 total) with a confocal microscope with a 60× objective, creating *z* stacks consisting of one image every 0.5 μm through each cell's thickness. Within each *z* stack, we created 2D grayscale projections by manually selecting images that most clearly showed the cell's SFs. We measured SF orientation using the custom software MatFiber, a MATLAB implementation of an intensity–gradient–detection algorithm originally developed by Karlon et al. (1) and subsequently used by our group to quantify collagen fiber orientation in histologic sections (2, 3) and by others to quantify SF alignment within stretched cells (4, 5). We used the orientations of structures within 6 × 6-pixel subregions to calculate the strength of alignment, $MVL^{SF}$ (ranging from zero, all SFs randomly oriented, to one, all SFs aligned) and MA, $MA^{SF}$ (Eqs. **2**–**4**). Then, the boundaries of each cell were traced to calculate each cell's $MA^{cell}$ and $MVL^{cell}$ as described above for comparison.

The calculated orientation of the cell using its boundary, $MA^{cell}$, and its SFs, $MA^{SF}$, correlated closely across most of the 60 cells analyzed, with an overall regression equation $MA^{cell} = 0.88 \times MA^{SF} - 7.2$ and an $R^2$ value of 0.84 (Fig. S1*A*). The strength of orientation of the cell using its boundary, $MVL^{cell}$, and its SFs, $MVL^{SF}$, was less tightly correlated on a cell by cell basis, with an $R^2$ value of 0.65 (Fig. S1*B*); the relationship between these two measures ($MVL^{cell} = 1.25 \times MVL^{SF} + 0.08$) suggested that MVL computed from the cell boundary is generally higher than the MVL computed from SFs imaged in the same cell.

### SI Modified Computational Model

Here, we briefly describe the model of Vigliotti et al. (6) and its application for the analysis of cells in tissues subjected to different boundary conditions as described in the text. We restrict attention to a 2D cell in the $x_1$–$x_2$ plane with the out of plane Cauchy stress $\Sigma_{33} = 0$.

### SI Configuration Under Static Loading

The model by Vigliotti et al. (6) describes the kinetics of SF remodeling for a given set of boundary conditions. The internal chemical kinetic processes (formation/dissociation of SFs and diffusion of the unbound SF proteins) are rapid and attain an equilibrium rapidly compared with the rate at which the cell can change its morphological configuration (i.e., its shape, size, etc.). Thus, under static loading conditions, the observed state is well-approximated by the equilibrium state of the cell. To determine that equilibrium state for a given set of boundary conditions, we use the model by Vigliotti et al. (6) to calculate the Gibbs free energy of the cell as outlined below.

Let $b_0$ be the thickness of the 2D cell in its elastic resting state and the corresponding volume $V_0$. The reference representative volume element (RVE) of the SFs within the cell in this resting configuration is assumed to be a cylinder of volume $V_R = \pi b_0 (n^R \ell_0/2)^2$, where $\ell_0$ is the length of an SF functional unit in its ground state and $n^R$ is the number of these ground-state functional units within the undeformed circular cell. The total number of functional unit packets within the cell is $N_0^T$, and we introduce $N_0 = N_0^T V_R/V_0$ as the average number of functional unit packets available per RVE; $N_0$ shall serve as a useful normalization parameter. The state of the SFs at location $x_i$ within the cell is described by their angular concentration $\eta(\phi, x_i)$ and the number $n(\phi, x_i)$ of the functional units in series along the length of each SF in the RVE, where $\phi$ is the angle with respect to the $x_1$ direction. Vigliotti et al. (6) argue that an applied stretch is shared equally among all subunits, so that the strain within each functional unit $\tilde{\varepsilon}_n$ is initially equal to the nominal strain $\varepsilon_n(x_i, \phi)$ in direction $\phi$. Subsequent addition or removal of subunits modifies the subunit stretch proportionally, so that, at steady state, the number $n^{ss}$ of functional units within the SFs is given by

$$\hat{n}^{ss} \equiv \frac{n^{ss}}{n^R} = \frac{[1 + \varepsilon_n(x_i, \phi)]}{1 + \tilde{\varepsilon}_n^{ss}}, \qquad \textbf{[S1]}$$

where $\tilde{\varepsilon}_n^{ss}$ is the strain at steady state within a functional unit of the SFs. To calculate the steady-state angular concentration of the SFs, we begin with the chemical potential of the functional units within the SFs as derived by Vigliotti et al. (6) as

$$\chi_b = \frac{\mu_b^{ss}}{n^R} + kT \ln\left[\left(\frac{\pi\hat{\eta}\,\hat{n}^{ss}}{\hat{N}_u}\right)^{\frac{1}{n^{ss}}}\left(\frac{\hat{N}_u}{\pi\hat{N}_L}\right)\right], \qquad \textbf{[S2]}$$

where $\hat{N}_u$ is the normalized concentration of the unbound SF proteins given by $\hat{N}_u \equiv N_u/N_0$ and $\hat{\eta} \equiv \eta n^R/N_0$ is the normalized angular density of SFs. Here, $\hat{N}_L$ is the number of available lattice sites, while the enthalpy of $n^R$ bound functional units at steady state is given in terms of the isometric SF stress $\sigma_{\max}$ and the internal energy $\mu_{b0}$ as

$$\mu_b^{ss} = \mu_{b0}\left[1 + \beta\left(\tilde{\varepsilon}_n^{ss}\right)^2\right] - \sigma_{\max}\left(1 + \tilde{\varepsilon}_n^{ss}\right)\Omega, \qquad \textbf{[S3]}$$

where $\Omega$ is the volume of $n^R$ functional units. The chemical potential of the unbound proteins in terms of the internal energy $\mu_u$ is

$$\chi_u = \frac{\mu_u}{n^R} + kT\,\ln\left(\frac{\hat{N}_u}{\pi\,\hat{N}_L}\right). \qquad \textbf{[S4]}$$

Equating the chemical potentials (Eqs. **S2** and **S4**) and denoting the steady-state values of $\hat{N}_u$ and $\hat{\eta}$ by $\hat{N}_u^{ss}$ and $\hat{\eta}^{ss}$, respectively, provide the following relation between these quantities:

$$\hat{\eta}^{ss}(x_i,\phi) = \frac{\hat{N}_u^{ss}}{\pi\,\hat{n}^{ss}(x_i,\phi)}\exp\left[\hat{n}^{ss}\,\frac{\mu_u - \mu_b^{ss}(x_i,\phi)}{kT}\right]. \qquad \textbf{[S5]}$$

We emphasize that $\hat{N}_u^{ss}$ is a constant [i.e., independent of $x_i$, as the chemical potential (Eq. **S4**) at equilibrium is constant over the entire cell]. We can now use conservation of the SF proteins to determine $\hat{N}_u^{ss}$. The normalized total number of functional unit packets $\hat{N}_T \equiv N_T/N_0$ in an RVE located at $x_i$ follows from the above analysis as

$$\hat{N}_T(x_i) = \hat{N}_u^{ss}(x_i)\left[1 + \frac{1}{\pi}\int_{-\frac{\pi}{2}}^{\frac{\pi}{2}}\exp\left[\hat{n}^{ss}\,\frac{\mu_u - \mu_b^{ss}(x_i,\phi)}{kT}\right]d\phi\right], \qquad \textbf{[S6]}$$

with conservation of the proteins then specifying

$$\frac{1}{A_0}\int_{A_0}\hat{N}_T\,dA = 1, \qquad \textbf{[S7]}$$

where $A_0 \equiv V_0/b_0$ is the resting area of the cell. Combining Eqs. **S6** and **S7**,

$$\hat{N}_u^{ss} = \frac{1}{1 + \frac{1}{A_0\pi}\int_{A_0}\int_{-\frac{\pi}{2}}^{\frac{\pi}{2}}\exp\left[\hat{n}^{ss}\,\frac{\mu_u - \mu_b^{ss}(x_i,\phi)}{kT}\right]d\phi\,dA}. \qquad \textbf{[S8]}$$

The cytoskeletal free energy is then

$$G_{cyto} = \frac{N_0 b_0}{V_R}\int_{A_0}\left[\hat{N}_u^{ss}\,\chi_u^{ss} + \int_{-\frac{\pi}{2}}^{\frac{\pi}{2}}\hat{\eta}\hat{n}\chi_b^{ss}\,d\phi\right]dA = \chi_u^{ss}N_0^T, \qquad \textbf{[S9]}$$

where $\chi_u^{ss}$ and $\chi_b^{ss}$ are the steady-state values of $\chi_u$ and $\chi_b$, respectively.

To complete the description of the cell, we need to specify the stress state. Vigliotti et al. (6) showed via a homogenization analysis that, in 2D, the stress state due to the active stresses generated by the SFs is given by

$$\begin{bmatrix}\sigma_{11} & \sigma_{12}\\ \sigma_{12} & \sigma_{22}\end{bmatrix} = f_0\sigma_{\max}\int_{-\pi/2}^{\pi/2}\hat{\eta}^{ss}[1+\varepsilon_n(\phi)]\begin{bmatrix}\cos^2\phi^* & \frac{\sin 2\phi^*}{2}\\ \frac{\sin 2\phi^*}{2} & \sin^2\phi^*\end{bmatrix}d\phi, \qquad \textbf{[S10]}$$

where $\phi^*$ is the angle of the SF measured with respect to $x_i$ and is related to $\phi$ by the rotation of the base vectors $e_i$ from the reference configuration; $f_0$ is the volume fraction of SF proteins under reference conditions. The total Cauchy stress $\Sigma_{ij}$ follows from an additive decomposition of $\sigma_{ij}$ and the passive stress $\sigma_{ij}^p$ as

$$\Sigma_{ij} = \sigma_{ij} + \sigma_{ij}^p. \qquad \textbf{[S11]}$$

The passive response is assumed to follow a compressible neo-Hookean relation of the form

$$W = \frac{E}{4(1+\nu)}\left[J^{-2/3}\sum_{j=1}^{3}\lambda_j^2 - 3\right] + \frac{E}{6(1-2\nu)}[J-1]^2, \qquad \textbf{[S12]}$$

where $E$ and $\nu$ are the Young's modulus and Poisson's ratio, respectively; $\lambda_j$ indicates the three principal stretches, and $J \equiv \lambda_1\lambda_2\lambda_3$. The principal components of the passive Cauchy stress are given as

$$\sigma_i^p \equiv \frac{\lambda_i}{J}\frac{\partial W}{\partial \lambda_i}. \qquad \textbf{[S13]}$$

The specification is complete by requiring mechanical equilibrium; that is,

$$\frac{\partial \Sigma_{ij}}{\partial x_j} = 0, \qquad \textbf{[S14]}$$

subject to the appropriate boundary conditions. The total free energy of the cell is then

$$G = G_{cyto} + b_0\int_{A_0} W dA, \qquad \textbf{[S15]}$$

which reduces to the expression

$$g \equiv g_{cyto} + g_{elas} = \rho_0\chi_u^{ss} + \frac{1}{A_0}\int_{A_0} W dA \qquad \textbf{[S16]}$$

for the free energy of the cell per unit volume. Here, $\rho_0 \equiv N_0^T/V_0$ is the volumetric concentration of the SF proteins, with $g_{cyto} \equiv \rho_0\chi_u^{ss}$ as the cytoskeletal free energy per unit volume and $g_{elas}$ as the corresponding elastic energy per unit volume.

Now consider the case of a low density of fibroblasts seeded in the gels or on 2D flat substrates, such that the cells do not directly interact with each other. The cells adhere to the collagen or other fibers in the gel or ligands on the substrate and remodel their shape and size so as to minimize their free energy. In the 2D context being analyzed here, we model the cells lying in the $x_1$–$x_2$ plane with $\Sigma_{33} = 0$. The gel is a weak, plastically deforming medium and thus, can only sustain stresses exerted by the cell

that are balanced by the applied boundary conditions. Furthermore, the local plastic deformation of the gel near each individual cell is unknown. We simplify the problem by modeling the cells to be spatially uniform, described by a single set of nominal strains $E_{11}, E_{22}$ and $E_{12}$. The above analysis to calculate the free energy of the cell then simplifies considerably with

$$\hat{N}_u^{ss} = \frac{1}{1 + \frac{1}{\pi}\int_{-\frac{\pi}{2}}^{\frac{\pi}{2}} \exp\left[\hat{n}^{ss}\,\frac{\mu_u - \mu_b^{ss}(x_i,\phi)}{kT}\right] d\phi} \qquad \text{[S17]}$$

and

$$g = \rho_0\left[\frac{\mu_u}{n^R} + kT\,\ln\left(\frac{\hat{N}_u^{ss}}{\pi\,\hat{N}_L}\right)\right] + g_{elas}, \qquad \text{[S18]}$$

where in this simplified setting, $g_{elas} = W$. The simulations were performed with the following set of parameters taken from Vigliotti et al. (6). All simulations are reported for cells at a temperature $T = 310$ K. The passive elastic parameters are taken to be $E = 5.0$ kPa and $\nu = 0.45$, while the maximum contractile stress $\sigma_{\max} = 240$ kPa and volume fraction $f_0 = 0.032$. The internal energies of the unbound and bound proteins are $\mu_u = 8\ k_B T_0$ and $\mu_{b0} = 9\ k_B T_0$, where $T_0 = 310$ K with $\beta = 1.2$, while the reference volume of $n^R$ functional units is taken to be $\Omega = 10^{-7.1}\mu\text{m}^3$. The volumetric concentration $\rho_0$ of the proteins was not specified in the work by Vigliotti et al. (6), as the free energy was not explicitly calculated. All simulations reported here use $\rho_0 = 1.5 \times 10^5\,\mu\text{m}^{-3}$.

We now proceed to detail the analysis for the three cases under consideration here: (*i*) biaxial constraint imposed on the gel, (*ii*) gels restrained uniaxially in the $x_1$ direction, and (*iii*) cells on stiff and flat 2D substrates. For the case of biaxial restraint, the applied boundary conditions can balance any stresses $\Sigma_{11}$ and $\Sigma_{22}$ generated by the cell, but the gel cannot sustain a shear stress $\Sigma_{12}$ generated by the cell. Thus, we constrain the cells to only assume states with $E_{12} = 0$, so that no elastic shear stresses are generated. Moreover, the boundary conditions in the $x_1$ and $x_2$ directions are identical, and thus, it is reasonable to assume that cells assume states with $E_{11} = E_{22}$. The cells then spread and remodel within the gel subject to these constraints to minimize their free energy $g$. We define normalized cytoskeletal and total free energies as

$$\hat{g}_{cyto} = \frac{g_{cyto} - \rho_0\mu_u / n^R + kT\ln(\pi\hat{N}_L)}{\rho_0\mu_u} = \frac{kT}{\mu_u}\ln\left(\hat{N}_u^{ss}\right) \qquad \text{[S19]}$$

and

$$\hat{g} = \frac{g - \rho_0\mu_u / n^R + kT\ln(\pi\hat{N}_L)}{\rho_0\mu_u} = \frac{kT}{\mu_u}\ln\left(\hat{N}_u^{ss}\right) + \hat{g}_{elas}, \qquad \text{[S20]}$$

respectively, where $\hat{g}_{elas} \equiv W/(\rho_0\mu_u)$. Here, we have subtracted $[\rho_0\mu_u/n^R - kT\ln(\pi\hat{N}_L)]$ in defining the normalized energies, as this term is a constant that does not vary with the state of the cell. A minimum is seen at $E_{11}^{opt} = E_{22}^{opt} = 0.062$; this represents the state that the cell assumes under static loading with this boundary condition (Fig. S1*A*), and the predicted distribution of assembled actin $\xi^{ss} \equiv \hat{\eta}^{ss}(\phi)\hat{n}^{ss}(\phi)$ is spatially isotropic (Fig. 3*I*). The configuration of cells under static loading on 2D flat substrates is identical to that for the biaxially constrained gel, as the 2D stiff substrates can support any stresses/tractions generated by the cell in the $x_1$ and $x_2$ directions.

For the case of uniaxial restraint in the $x_1$ direction, equilibrium requires that resultant forces in the $x_2$ direction vanish, and therefore, we only allow the cells to assume states with $\Sigma_{22} = 0$. As in the biaxial case, we also assume that the gel cannot support shear stresses $\Sigma_{12}$, so that $E_{12} = 0$. Thus, the problem reduces to determining the value of $E_{11}$ that minimizes $\hat{g}$. A minimum is seen at $E_{11}^{opt} = 0.075$, $E_{22}^{opt} = -0.2107$ (Fig. S1 *B* and *C*) and is associated with preferential alignment of SFs along the $x_1$ direction (Fig. 3 *C* and *F*).

## SI Analysis of Fibroblast-Populated Gels Under Cyclic Loading

To simulate cyclic loading of cells (on 2D substrates and in gels), we separate the strain $E_{ij}$ of the cell into two parts: a static time-independent component $\bar{E}_{ij}$ and a cyclic component $\Delta E_{ij}(t)$, such that $E_{ij}(t) = \bar{E}_{ij} + \Delta E_{ij}(t)$. We assume that, over long timescales, the cells can remodel, such that they adjust their connection to the gel or the substrate and adjust $\bar{E}_{ij}$ so as to minimize their free energy subject to the appropriate boundary conditions. Thus, the calculation of $\bar{E}_{ij}$ reduces to the free energy minimization of the cell under equivalent static boundary conditions as outlined above. It now remains to specify the response of cells subject to the additional time-dependent strains $\Delta E_{ij}(t)$.

The cyclic analysis of the cells in the gels differed from that for cells on the 2D substrates. Cells on 2D substrates are adhered to the substrates, and the cyclic strains $\Delta e_{ij}(t)$ applied to the substrate are directly transmitted to the cell [i.e., $\Delta E_{ij}(t) = \Delta e_{ij}(t)$]. However, for cells within very soft 3D gels, the majority of the imposed strains are accommodated within the gel, with only a small fraction $\delta$ transmitted to the cells (7) [i.e., $\Delta E_{ij}(t) = \delta\,\Delta e_{ij}(t)$, where $0 \le \delta \le 1$].

We analyze the three cyclic loading cases using the full model by Vigliotti et al. (6) (i.e., the model accounting for transient evolution of the cytoskeleton and not just the steady-state limit as described above). The three cyclic loading cases and the associated boundary conditions are as follows.

*i*) Cyclic response of cells on 2D substrates: here, we impose $\Delta E_{11}(t) = \Delta e_{11}(t)$ with $\Delta E_{22}(t) = 0$.
*ii*) Strip uniaxial stretch of cells in gels: here, we impose $\Delta E_{11}(t) = \delta\Delta e_{11}(t)$ with $\Delta E_{22}(t) = 0$.
*iii*) Uniaxial stretch of cells in gels: here, we impose $\Delta E_{11}(t) = \delta\Delta e_{11}(t)$ with $\Sigma_{22}(t) = 0$.

The transient model of Vigliotti et al. (6) requires a few additional parameters to those specified above. These are taken from ref. 6, but we list them here for the sake of completeness. The activation barrier for SF kinetics is taken to be $\mu_a = 20\ k_B T_0$, while the time constant for SF formation/dissociation is $\omega_n = 20$ Hz, with the SF remodeling assumed to be slow with a rate constant $\alpha = 0.01$ Hz. In addition, we now need to specify the parameters for the dependence of the stress generated by the SFs on the SF strain rates, which are assumed to have a Hill-like form with associated constants $\dot{\varepsilon}_0 = 0.53\ \text{s}^{-1}$, $\varepsilon_p = 0.6$, and $\varepsilon_s = 0.3$. The cyclic simulations were performed with initial conditions given by the corresponding static analysis described above. Finally, the parameter $\delta$ that sets the cyclic strain transmitted into the cells in the gels was set to $\delta = 0.0125$ in all simulations reported here. Cyclic loading was imposed until a steady state was attained, which was realized for all boundary conditions after ~12 h of cyclic loading. The cyclic steady-state distributions of $\xi \equiv \eta n$ as a function of $\phi$ are presented in Fig. 3 *C*, *F*, and *I*.

1. Karlon WJ, Covell JW, McCulloch AD, Hunter JJ, Omens JH (1998) Automated measurement of myofiber disarray in transgenic mice with ventricular expression of ras. *Anat Rec* 252:612–625.
2. Fomovsky GM, Holmes JW (2010) Evolution of scar structure, mechanics, and ventricular function after myocardial infarction in the rat. *Am J Physiol Heart Circ Physiol* 298: H221–H228.
3. Holmes JW (2015) MatFiber version of Fiber3 algorithm for automated fiber orientation analysis. Cardiac Biomechanics Group. Available at bme.virginia.edu/holmes/downloads/index.html. Accessed April 10, 2015.
4. Kaunas R, Nguyen P, Usami S, Chien S (2005) Cooperative effects of Rho and mechanical stretch on stress fiber organization. *Proc Natl Acad Sci USA* 102:15895–15900.
5. Karlon WJ, et al. (1999) Measurement of orientation and distribution of cellular alignment and cytoskeletal organization. *Ann Biomed Eng* 27:712–720.
6. Vigliotti A, Ronan W, Baaijens FPT, Deshpande VS (2016) A thermodynamically motivated model for stress-fiber reorganization. *Biomech Model Mechanobiol* 15:761–789.
7. Ujihara Y, et al. (2015) Computational studies on strain transmission from a collagen gel construct to a cell and its internal cytoskeletal filaments. *Comput Biol Med* 56: 20–29.

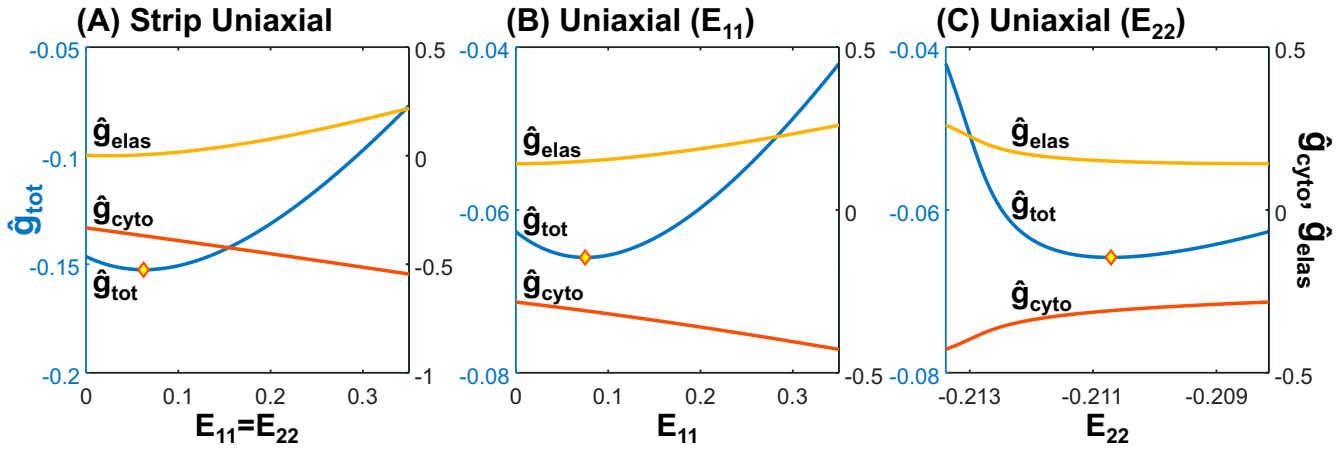


**Fig. S1.** Modified computational model minimizes free energy ($\hat{g}_{tot} = \hat{g}_{cyto} + \hat{g}_{elas}$) based on the boundary conditions to determine equilibrium cell strain. (*A*) When the $x_2$ direction was constrained (strip uniaxial cases), SFs reached the same minimum free energy and cell strain in all directions ($E_{11} = E_{22}$). (*B* and *C*) When the $x_2$ direction was free (uniaxial cases), SFs in $x_2$ (*C*) reached minimum free energy (yellow diamond) at a cell strain much lower than in $x_1$ (*B*).

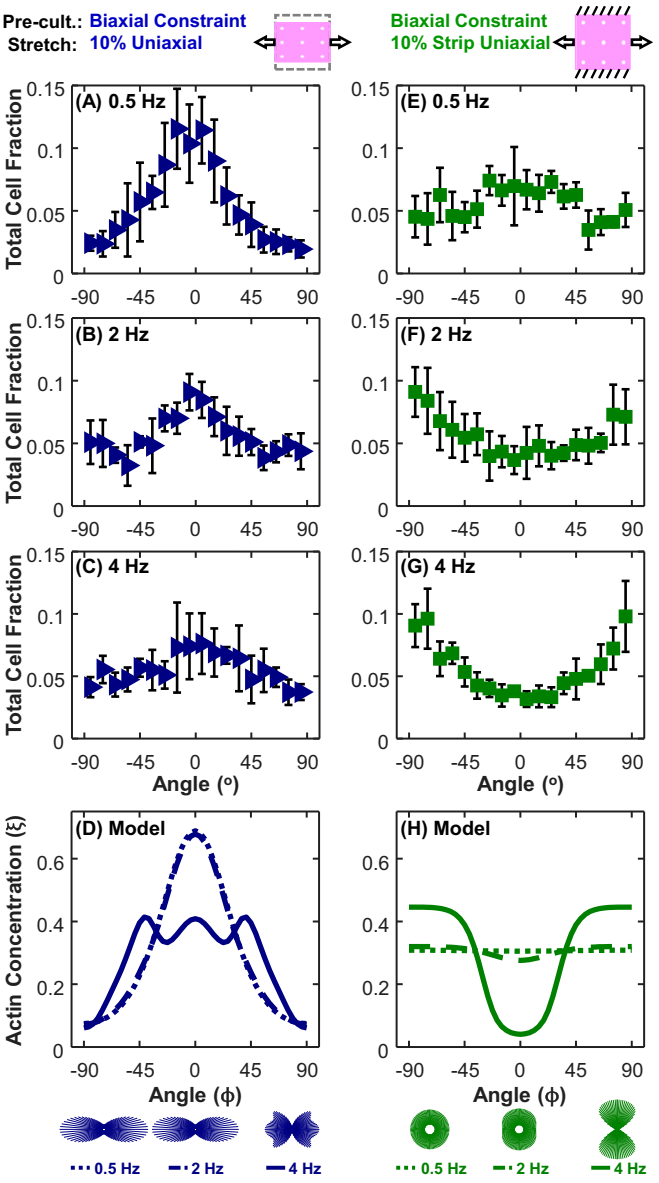


**Fig. S2.** Angular histograms of cell orientation for 10% uniaxial cyclic stretch (*A*–*C*) and 10% strip uniaxial cyclic stretch (*E*–*G*) at 0.5, 2, and 4 Hz after 72 h. Each data point is representative of five independent experiments (except uniaxial 4 Hz; $n = 4$) and expressed as the mean ± SD. Angular histograms of SF orientation simulations for uniaxial (*D*, *Upper*) and strip uniaxial (*H*, *Upper*) conditions across our range of frequencies (dotted lines, 0.5 Hz; dashed lines, 2 Hz; solid lines, 4 Hz). *D*, *Lower* and *H*, *Lower* show circular histogram representations of these SFs.

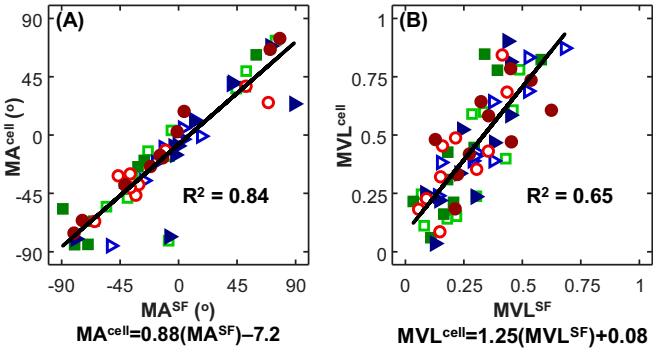


**Fig. S3.** The orientation of SFs within 10 cells from each stretch condition (60 total; symbols correspond with those in Figs. 2 and 3) correlated strongly with the orientation of the entire cell. (*A*) Orientation of the SFs ($MA^{SF}$) vs. tracing its boundary ($MA^{cell}$). (*B*) Comparison of the strength of alignment of the cell using its SFs ($MVL^{SF}$) vs. the alignment of the cell using its boundary ($MVL^{cell}$).

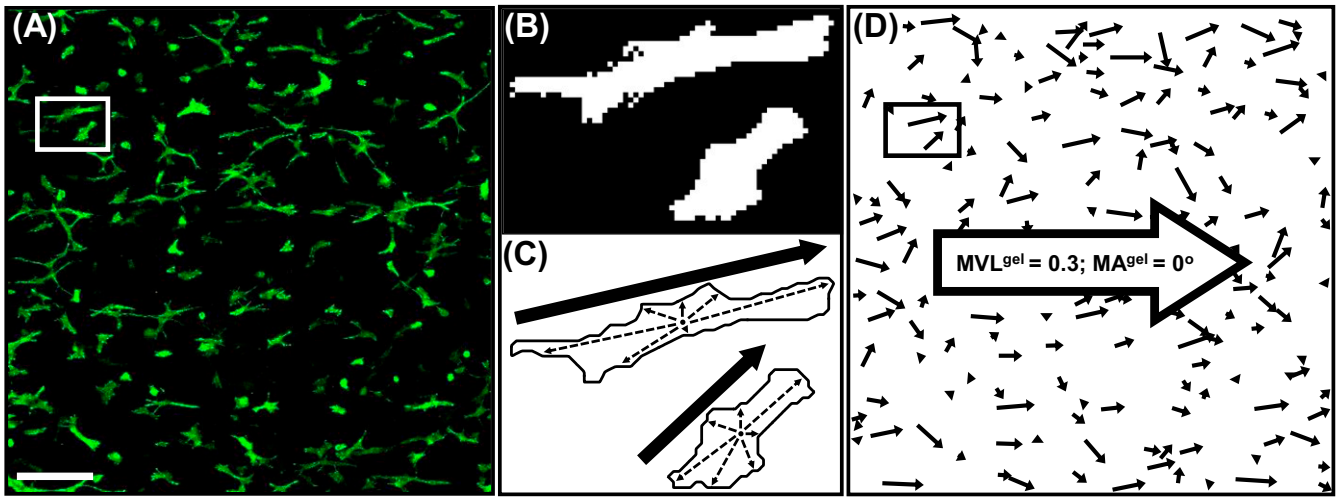


**Fig. S4.** Quantification of cell alignment. (*A*) A representative 2D projection of F actin-stained adult rat cardiac fibroblasts taken from the core of the tissue. (Scale bar: 200 μm.) (*B*) Magnification of the boxed region in *A* converted into a binary image. (*C*) Vectors (dashed arrows represent a subset of the 400 vectors used) drawn from the centroid (dots) to the boundary of the cell were used to calculate the cell's strength of alignment ($MVL^{cell}$; ranging from zero, a circular cell, to one, a highly aligned, spindly cell) and orientation ($MA^{cell}$; thick black arrows). The top cell, which is longer and more highly aligned, has a higher $MVL^{cell}$ ($MVL^{cell} = 0.85$; $MA^{cell} = 13°$) than the bottom cell ($MVL^{cell} = 0.55$; $MA^{cell} = 43°$). (*D*) The mean vectors of all cells in *A* are saved and plotted. These vectors were used to then calculate each gel's overall MVL ($MVL^{gel}$; ranging from zero, cells randomly aligned, to one, all cells strongly aligned in the same direction) and MA ($MA^{gel}$). In this image, the cells are aligned in the 0° ($x_1$) direction with moderate strength.